UNCERTAINTIES 2012

Proceedings of the 1st International Symposium on Uncertainty Quantification and Stochastic Modeling
February 26th to March 2nd, 2012, Maresias, São Sebastião, SP, Brazil

ON THE DYNAMICS OF A NONLINEAR CONTINUOUS RANDOM SYSTEM

Americo Barbosa da Cunha Junior, Rubens Sampaio

Department of Mechanical Engineering, PUC–Rio
Rua Marquês de São Vicente, 225, Gávea, Rio de Janeiro - RJ, Brasil - 22453-900
{americo,rsampaio}@puc-rio.br

Abstract. *The dynamics of a mechanical system shows dependence on parameters such as physical and geometrical properties, initial and boundary conditions, etc. In a deterministic system all of these parameters are fixed and a single set of differential equations completely describes the system behavior. However, in a stochastic system one or more of these parameters are random and there is a set of differential equations associated with it (one for each realization of the system). Thus, to characterize the dynamics of a random system, it is necessary to employ methods for stochastic computations. This work studies the dynamics of one-dimensional elastic bar, with random elastic modulus and prescribed boundary conditions, say, fixed at one end and attached to two springs (one linear and another nonlinear) fixed at a rigid wall. The system analysis assumes that the elastic modulus has gamma probability distribution and uses Monte Carlo simulations to compute the propagation of uncertainties for the bar displacement. After describing the deterministic and stochastic modeling of the bar, two configurations of the stochastic model are analyzed to characterize the effect of nonlinearity on the overall behavior of this mechanical system. The results indicate that nonlinearity tends to affect more the spatial behavior of the elastic bar than its temporal behavior.*

Keywords. *nonlinear dynamics, stochastic model, stochastic simulation, uncertainty quantification.*

1 INTRODUCTION

The dynamics of a mechanical system depends on some parameters such as physical and geometrical properties, constraints, external and internal loading, initial and boundary conditions. Most of the theoretical models used to describe the behavior of a mechanical system assume nominal values for these parameters, such that the model gives one response for a given particular input. In this case the system is *deterministic* and its behavior is described by a single set of differential equations. However, in real systems they do not have a fixed value since they are subjected to uncertainties of measurement, imperfections in manufacturing processes, change of properties, etc. This variability in the set of system parameters leads to a large number of possible system responses for a given particular input. Now the system is *stochastic* and there is a family of differential equations sets (one for each realization of the random system) associated to it. Thus, to characterize the dynamics of a random system, it is necessary to employ methods for stochastic computations.

In order to simulate the dynamics of a random system, one possibility is to use Monte Carlo (MC) simulations. In this method, an ensemble of realizations of the random system is obtained and then statistics of it are computed. This method was originally proposed by Metropolis and Ulam (1949) and is well explained in Shonkwiler and Mendivil (2009).

The MC method does not requires that one implements a new computer code to simulate a random dynamical system. If a deterministic code to simulate a similar system is available, the stochastic simulation can be performed by running the deterministic program several times, changing only the random parameters. This nonintrusive characteristic is a great advantage of MC when compared to other methods such as generalized Polynomial Chaos (gPC), (Xiu and Karniadakis, 2002), which demands a new code each new random system that one wants to simulate. Also, if MC simulation is performed for a large number of samples, it completely describes the statistical behavior of the random system. Unfortunately the MC is a very time-consuming method.

This paper is a first effort to study the nonlinear dynamics of a one-dimensional elastic bar, subject to a series of randomness (system parameters, external forcing, boundary and initial conditions). In this sense, this work considers a bar with random elastic modulus and prescribed boundary conditions, say, fixed at one end and attached to two springs (one linear and another nonlinear) fixed at a rigid wall.

A detailed discussion of the deterministic modeling of the problem (physical model, strong and weak formations, orthogonality relation between the shape modes), of the discretization method and of the algorithm used to solve the equation of interest is presented. In the stochastic modeling section, the principle of maximum entropy (Shannon, 1948; Jaynes, 1957a,b) is used to construct a probability distribution for the elastic modulus. Since the stochastic problem under consideration presents a relative low level of complexity, the MC method is chosen to assess it and due to its simplicity and effectiveness. Two configurations of the model are analyzed in order to characterize the effect of nonlinearity, introduced in the model by the boundary condition.

2 DETERMINISTIC APPROACH

This section presents the deterministic modeling (physical and mathematical) of a elastic bar, discusses the problem of obtaining the bar normal modes, the discretization of the model equation and numerical procedure adopted to solve the resulting nonlinear equation.

2.1 Physical model

The continuous system of interest is a one-dimensional elastic bar, in which the elasticity is characterized by the elastic modulus E. This bar has constant mass density ρ, constant circular cross section area A and its unstretched length is L. The left side of the bar is fixed at a rigid wall while the right side is attached to two springs fixed at a rigid wall. The first spring (of rigidity k_1) is linear and exerts a restoring force proportional to the stretching on the bar. The second spring (of rigidity k_2) is nonlinear and its restoring force is proportional to the cube of the stretching. The displacement of a point x of the bar at a time t is denoted by $u(x,t)$. In the bar also acts an external force, which depends on x and t, denoted by $f(x,t)$. Initially, any point x of the bar presents a displacement $u_0(x)$ and a velocity $v_0(x)$. This continuous system is sketched in Fig. 1 below.

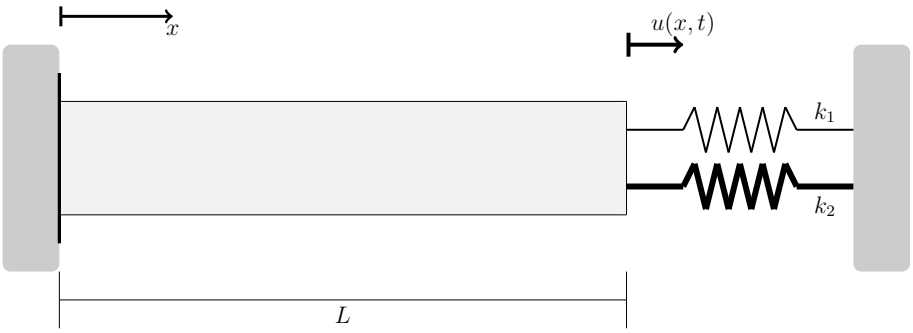

Figure 1: Sketch of a bar fixed at one and attached to two springs on the other extreme.

2.2 Mathematical model

The strong and variational formulations of the problem that describes the dynamics of the bar are shown below.

2.2.1 strong formulation

The strong formulation of the problem under study starts with an equation of motion of the bar and the constitutive laws. In this way, it is possible to show that u evolves according to the following partial differential equation (PDE), valid for $0 < x < L$ and $0 < t < +\infty$,

$$\rho A \frac{\partial^2}{\partial t^2} u(x,t) = \frac{\partial}{\partial x}\left(EA \frac{\partial}{\partial x} u(x,t) \right) + f(x,t). \tag{1}$$

Also, the bar is fixed at one end and subjected to linear and nonlinear restoring forces (from the springs) at the other extreme. These boundary conditions, for $0 \leq t < +\infty$, can be written as

$$u(0,t) = 0 \qquad \text{and} \qquad EA \frac{\partial}{\partial x} u(L,t) = -k_1 u(L,t) - k_2 \left[u(L,t) \right]^3. \tag{2}$$

It is also assumed that, for $0 \leq x \leq L$, the initial position and the initial velocity of the bar are known functions of x, given by

$$u(x,0) = u_0(x) \qquad \text{and} \qquad \frac{\partial}{\partial t} u(x,0) = v_0(x). \tag{3}$$

2.2.2 variational formulation

First a class of (weight) functions w is defined by the following set

$$W = \left\{ w : [0,L] \to \mathbb{R} \;\; \middle| \;\; \int_0^L w(x)^2 dx < +\infty \;\; \text{and} \;\; w(0) = 0 \right\}.$$

Then, the residual function (left hand side minus right hand side) of Eq.(1) is multiplied by w, and integrated over the interval $[0,L]$.

After that, integration by parts is used to incorporates on the formulation the boundary condition given by the second part of Eq.(2), to yield

$$\mathscr{M}(u,w)+\mathscr{K}(u,w)=\mathscr{F}(w)+\mathscr{G}(u,w), \tag{4}$$

where $\mathscr{M}$ is the mass operator; $\mathscr{K}$ is the stiffness operator; $\mathscr{F}$ is the external force operator; and $\mathscr{G}$ is the nonlinear force operator; respectively, defined as

$$\mathscr{M}(u,w)=\int_0^L \rho A \frac{\partial^2}{\partial t^2}u(x,t)w(x)dx, \tag{5}$$

$$\mathscr{K}(u,w)=\int_0^L EA\frac{\partial}{\partial x}u(x,t)\frac{\partial}{\partial x}w(x)dx+k_1u(L,t)w(L), \tag{6}$$

$$\mathscr{F}(w)=\int_0^L f(x,t)w(x)dx, \tag{7}$$

and

$$\mathscr{G}(u,w)=-k_2\left[u(L,t)\right]^3 w(L). \tag{8}$$

The variational formulations for the initial conditions of Eq.(3) are obtained by the same way, and given by

$$\int_0^L \rho A u(x,0)w(x)dx=\int_0^L \rho A u_0(x)w(x)dx, \tag{9}$$

and

$$\int_0^L \rho A \frac{\partial}{\partial t}u(x,0)w(x)dx=\int_0^L \rho A v_0(x)w(x)dx, \tag{10}$$

respectively.

2.3 An eigenvalue problem

This sections presents the formulation and solution of an eigenvalue value problem, associated to the problem described in section 2.2 and explore two relations of orthogonality.

2.3.1 eigenvalues and eigenfunctions

Initially, consider the homogeneous equation associated to the variational formulation of Eq.(4),

$$\mathscr{M}(u,w)+\mathscr{K}(u,w)=0. \tag{11}$$

Now assume that the above equation has a solution of the form $u(x,t)=e^{i\nu t}\phi(x)$, where ν is the natural frequency, ϕ is shape mode and i is the imaginary unit ($\sqrt{-1}$). Replacing the expression of u above in the Eq.(11) and using the linearity of the operators $\mathscr{M}$ and $\mathscr{K}$, one gets

$$\left[-\nu^2\mathscr{M}(\phi,w)+\mathscr{K}(\phi,w)\right]e^{i\nu t}=0. \tag{12}$$

Since $e^{i\nu t}\neq 0$ for all t, the last equation is equivalent to

$$-\nu^2\mathscr{M}(\phi,w)+\mathscr{K}(\phi,w)=0. \tag{13}$$

The Equation (13) defines a generalized eigenvalue problem. To solve it, the technique of separation of variables is employed, which leads to a Sturm-Liouville problem (Al Gwaiz, 2007), with denumerable number of solutions. Therefore, this generalized eigenvalue problem has a denumerable number of solutions, all of then such as the following eigenpair (ν_n^2,ϕ_n), where ν_n is the n-th bar natural frequency and ϕ_n is the n-th bar shape mode.

It is important to observe that, the eigenfunctions $\{\phi_n\}_{n=1}^{+\infty}$ span the space of functions which contains the solution of the Eq.(13) (Brezis, 2010). These eigenfunctions possess two interesting relations of orthogonality, that are explored below.

2.3.2 orthogonality relations

Now consider the pairs (ν_n^2, ϕ_n) and (ν_m^2, ϕ_m), such that $\nu_m \neq \nu_n$, that are solutions of Eq.(13). So, it is true that

$$-\nu_n^2 \mathscr{M}(\phi_n, w) + \mathscr{K}(\phi_n, w) = 0, \tag{14}$$

and

$$-\nu_m^2 \mathscr{M}(\phi_m, w) + \mathscr{K}(\phi_m, w) = 0. \tag{15}$$

Moreover, as the Eqs.(14) and (15) are valid for all $w \in W$, one can chose $w = \phi_m$ on the former and $w = \phi_n$ on the latter, so that the following equations are obtained

$$-\nu_n^2 \mathscr{M}(\phi_n, \phi_m) + \mathscr{K}(\phi_n, \phi_m) = 0, \tag{16}$$

and

$$-\nu_m^2 \mathscr{M}(\phi_m, \phi_n) + \mathscr{K}(\phi_m, \phi_n) = 0. \tag{17}$$

Due to the symmetry of the operators $\mathscr{M}$ and $\mathscr{K}$, the last two equations are equivalent to

$$-\nu_n^2 \mathscr{M}(\phi_n, \phi_m) + \mathscr{K}(\phi_n, \phi_m) = 0, \tag{18}$$

and

$$-\nu_m^2 \mathscr{M}(\phi_n, \phi_m) + \mathscr{K}(\phi_n, \phi_m) = 0. \tag{19}$$

Now, subtract Eq.(18) from Eq.(19) to get

$$\left(\nu_n^2 - \nu_m^2\right) \mathscr{M}(\phi_n, \phi_m) = 0, \tag{20}$$

and use the fact that $\nu_n \neq \nu_m$ to obtain

$$\mathscr{M}(\phi_n, \phi_m) = 0. \tag{21}$$

Finally, as a consequence of the Eqs.(14) and (21), one obtains

$$\mathscr{K}(\phi_n, \phi_m) = 0. \tag{22}$$

The last two equations define the orthogonality relations between the bar shape modes. They are good choices for the basis function when a weighted residual procedure (Finlayson and Scriven, 1966) is used to approximate the solution of a nonlinear variational equation, such as Eq.(4).

According to Blevis (1993), a bar, fixed at one end, and attached to a linear spring on the other (fixed-spring bar), has natural frequencies and the orthogonal shape modes given by

$$\nu_n = \lambda_n \frac{c}{L}, \tag{23}$$

and

$$\phi_n(x) = \sin\left(\lambda_n \frac{x}{L}\right), \tag{24}$$

where $c = \sqrt{E/\rho}$ and the λ_n are the solutions of

$$\cot(\lambda_n) + \left(\frac{k_1 L}{AE}\right) \frac{1}{\lambda_n} = 0. \tag{25}$$

The Figure 2 illustrates the first nine orthogonal shape modes of the fixed-spring bar, and each sub-caption indicates the approximated natural frequency associated with the corresponding mode.

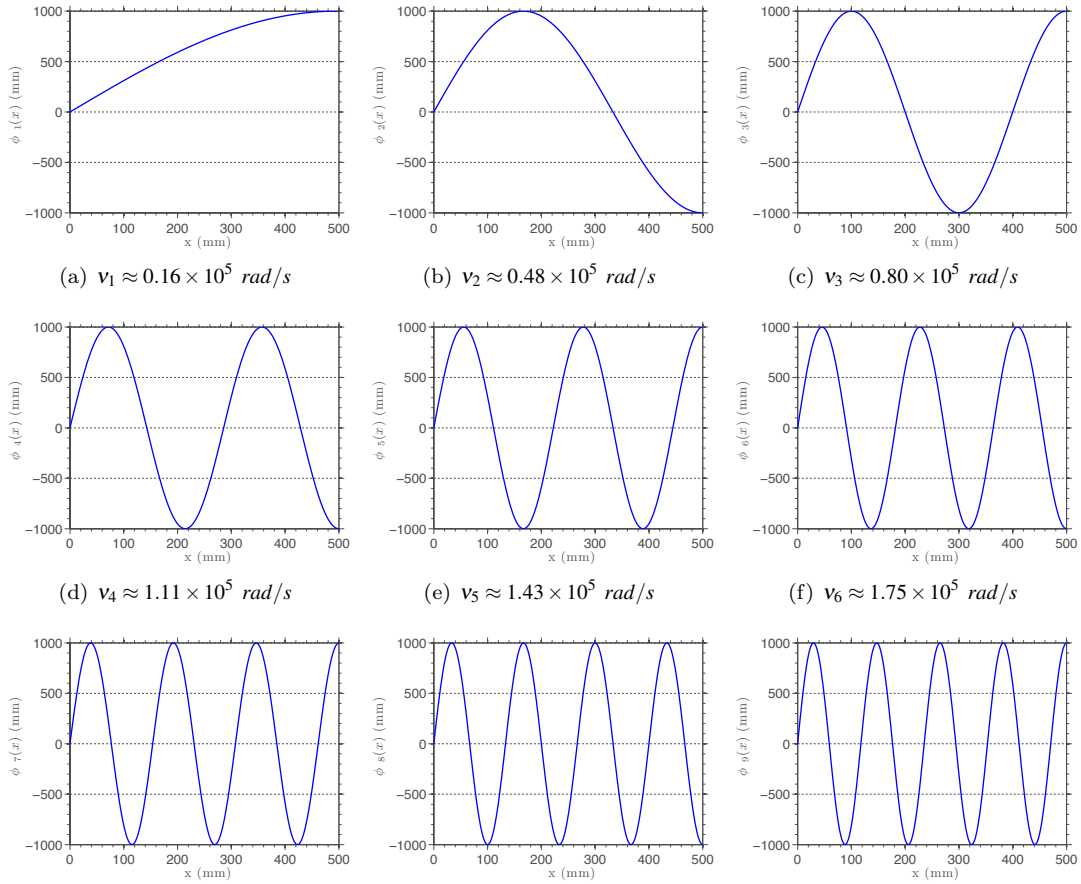

(a) $\nu_1 \approx 0.16 \times 10^5$ *rad/s* (b) $\nu_2 \approx 0.48 \times 10^5$ *rad/s* (c) $\nu_3 \approx 0.80 \times 10^5$ *rad/s*

(d) $\nu_4 \approx 1.11 \times 10^5$ *rad/s* (e) $\nu_5 \approx 1.43 \times 10^5$ *rad/s* (f) $\nu_6 \approx 1.75 \times 10^5$ *rad/s*

(g) $\nu_7 \approx 2.07 \times 10^5$ *rad/s* (h) $\nu_8 \approx 2.39 \times 10^5$ *rad/s* (i) $\nu_9 \approx 2.71 \times 10^5$ *rad/s*

Figure 2: The first nine orthogonal shape modes and the corresponding (approximated) natural frequencies of a fixed-spring bar.

2.4 Model equation discretization

In order of approximate the solution of Eqs.(4), (9) and (10) the Galerkin method (Hughes, 2000) is employed. In this weighted residual method, the same class of functions is used to construct the basis and weight functions. Also, the displacement field u is approximated by a linear combination of the form

$$u^N(x,t) = \sum_{n=1}^{N} U_n(t)\phi_n(x), \tag{26}$$

where the basis functions ϕ_n are the orthogonal shape modes of the fixed-spring bar, exemplified in the end of section 2.3, and the coefficients U_n are time-dependent functions. For a reason that will be clear soon, define $\mathbf{U}(t)$ of $\mathbb{R}^N$ as the vector in which the n-th component is the $U_n(t)$.

Since u^N is not a solution of Eq.(4), when the field u is approximated by u^N, a residual function is obtained. This residual function is orthogonally projected into the vector space spanned by the functions $\{\phi_n\}_{n=1}^N$ in order to minimize the error incurred by the approximation (Hughes, 2000). This procedure results in the following $N \times N$ set of nonlinear ordinary differential equations (ODEs)

$$[M]\ddot{\mathbf{U}}(t) + [K]\mathbf{U}(t) = \mathbf{F}(t) - \mathbf{G}\left[\mathbf{U}(t)\right], \tag{27}$$

supplemented by the following pair of initial conditions

$$\mathbf{U}(0) = \mathbf{U}_0 \qquad \text{and} \qquad \dot{\mathbf{U}}(0) = \mathbf{V}_0. \tag{28}$$

In Equation (27), $[M]$ is the mass matrix, $[K]$ is the stiffness matrix, and the upper dot denotes the time derivative. Also, $\mathbf{F}(t)$ and $\mathbf{G}\left[\mathbf{U}(t)\right]$ are vectors of $\mathbb{R}^N$, which respectively represent the external force and the nonlinear force vectors. Each one of these objects is a finite dimensional representation of the operators in the variational equation, Eq.(4). They are obtained when one replace in Eq.(4), u by u^N, w by ϕ_n $(n=1,\cdots,N)$ and then take into account the linear properties of $\mathscr{M}$ and $\mathscr{K}$. In terms of components, these finite dimensional objects are, respectively, given by

$$M_{mn} = \int_0^L \rho A \phi_n(x)\phi_m(x)dx, \tag{29}$$

$$K_{mn} = \int_0^L EA \tfrac{\mathrm{d}}{\mathrm{d}x}\phi_n(x)\tfrac{\mathrm{d}}{\mathrm{d}x}\phi_m(x)dx + k_1\phi_n(L)\phi_m(L), \tag{30}$$

$$F_m = \int_0^L f(x,t)\phi_m(x)dx, \tag{31}$$

and

$$G_m = -k_2\left[\sum_{n=1}^{N} U_n(t)\phi_n(L)\right]^3 \phi_m(L). \tag{32}$$

Regarding the initial conditions $\mathbf{U}(0)$ and $\dot{\mathbf{U}}(0)$, the first orthogonality relation of the shape modes, Eq.(21), makes their components, respectively, equal to

$$U_m(0) = \frac{\displaystyle\int_0^L \rho A u_0(x)\phi_m(x)dx}{\displaystyle\int_0^L \rho A\left[\phi_m(x)\right]^2 dx}, \tag{33}$$

and

$$\dot{U}_m(0) = \frac{\displaystyle\int_0^L \rho A v_0(x)\phi_m(x)dx}{\displaystyle\int_0^L \rho A\left[\phi_m(x)\right]^2 dx}. \tag{34}$$

2.5 Nonlinear ODE system solution

Let $t_n = n\Delta t$ be a temporal mesh defined over the interval $[0,T]$, with an uniform time step Δt.

In order to solve the initial value problem of Eqs.(27) and (28), the Newmark method (Newmark, 1959) defines the following integration scheme

$$\mathbf{v}_{n+1} = \mathbf{v}_n + (1-\gamma)\Delta t\,\mathbf{a}_n + \gamma\Delta t\,\mathbf{a}_{n+1}, \tag{35}$$

$$\mathbf{d}_{n+1} = \mathbf{d}_n + \Delta t\,\mathbf{v}_n + \left(\frac{1}{2}-\beta\right)\Delta t^2\mathbf{a}_{n+1}, \tag{36}$$

where $\mathbf{d}_n$, $\mathbf{v}_n$ and $\mathbf{a}_n$ are approximations to $\mathbf{U}(t_n)$, $\dot{\mathbf{U}}(t_n)$ and $\ddot{\mathbf{U}}(t_n)$, respectively. The parameters γ and β are associated with the accuracy and stability of the scheme. For details about the convergence and stability of the method, the interested reader may consult Hughes (2000).

The nonlinear initial value problem of Eqs.(27) and (28) together with the Newmark scheme, Eqs.(35) and (36), defines a nonlinear problem of algebraic equations with unknowns $\mathbf{d}_n$, $\mathbf{v}_n$ and $\mathbf{a}_n$. This system is solved using the Newton-Rapson method, which defines the following iterative process in k

$$\mathbf{a}_{n+1}^{(k+1)} = \mathbf{a}_{n+1}^{(k)} + \frac{1}{\beta\Delta t^2}\Delta\mathbf{d}, \tag{37}$$

$$\mathbf{v}_{n+1}^{(k+1)} = \mathbf{v}_{n+1}^{(k)} + \frac{\gamma}{\beta\Delta t}\Delta\mathbf{d}, \tag{38}$$

$$\mathbf{d}_{n+1}^{(k+1)} = \mathbf{d}_{n+1}^{(k)} + \Delta\mathbf{d}, \tag{39}$$

where $\Delta\mathbf{d}$ is the solution of the following linear system of algebraic equations

$$\left(\frac{1}{\beta\Delta t^2}\frac{\partial\mathbf{r}}{\partial\mathbf{a}} + \frac{\gamma}{\beta\Delta t}\frac{\partial\mathbf{r}}{\partial\mathbf{v}} + \frac{\partial\mathbf{r}}{\partial\mathbf{d}}\right)\Delta\mathbf{d} = -\mathbf{r}\left(\mathbf{a}^*, \mathbf{v}^*, \mathbf{d}^*\right) \tag{40}$$

being the residual vector $\mathbf{r}$ defined by

$$\mathbf{r}(\mathbf{a}, \mathbf{v}, \mathbf{d}) = [M]\,\mathbf{a} + [K]\,\mathbf{d} - \mathbf{F}(t) + \mathbf{G}(\mathbf{d}). \tag{41}$$

The linear system of Eq.(40) is obtained when one replace Eqs.(37), (38) and (39) in the linear approximation of $\mathbf{r}$ around the initial guess $\left(\mathbf{a}^*, \mathbf{v}^*, \mathbf{d}^*\right)$.

In practical terms, this procedure continues until the 2-norm of the residual vector becomes less than a specified tolerance ε, i.e., until

$$\|\mathbf{r}\|_2 < \varepsilon. \tag{42}$$

All the simulations reported in this work use $\gamma = 1/2$, $\beta = 1/12$, and $\varepsilon = 10^{-7}$.

3 STOCHASTIC APPROACH

This section presents the stochastic modeling of the continuous elastic bar described in section 2.1 when the elastic modulus is a random parameter.

3.1 Probabilistic model

The elastic modulus of the bar has a random nature, so that the theory of probability (Papoulis and Pillai, 2002) can be applied.

Consider a probability space $(\Omega, \mathbb{A}, \mathbb{P})$, where Ω is sample space, $\mathbb{A}$ is a σ-field over Ω and $\mathbb{P}$ is a probability measure. Working in this probabilistic space, the elastic modulus is assumed to be a random variable that, associates to each event $\omega \in \Omega$ a real number $E(\omega)$. In this sense, the displacement of the bar is the random field $U : \Omega \times [0, L] \times [0, +\infty) \to \mathbb{R}$, which evolves according the following stochastic partial differential equation (SPDE)

$$\rho A\frac{\partial^2}{\partial t^2}U(\omega, x, t) = \frac{\partial}{\partial x}\left(E(\omega)A\frac{\partial}{\partial x}U(\omega, x, t)\right) + f(x, t) - k_2\left[U(\omega, x, t)\right]^3\delta(x - L), \tag{43}$$

being the partial derivatives now defined in the mean square sense (Papoulis and Pillai, 2002). This problem has boundary and initial conditions similar to those defined in Eqs.(2) and (3), by changing u for U only.

3.2 Elastic modulus distribution

The choice of a probability distribution for the elastic modulus cannot be arbitrary. All information available about this parameter must be taken into account before one defines its distribution. In this sense, the work of Soize (2000) suggests the use of the maximum entropy principle (Shannon, 1948; Jaynes, 1957a,b) to obtain the desired probability distribution. To the best of the authors knowledge, a distribution obtained this way is the one that most accurately describes the current knowledge about the random parameter.

The elastic modulus cannot be negative, so it is reasonable to assume the support of E as the interval $(0, +\infty)$. Also, the mean value of E is specified. Finally, one also wants that the displacement of the bar has finite variance. Respecting the above constraints, the probability density function (PDF) with maximum entropy is that one which corresponds to the gamma distribution (Kapur and Kesavan, 1992). Therefore, from now on, it is assumed that the random variable E is gamma distributed, with mean parameter $\mu_E = 203\ GPa$ and dispersion factor $\delta_E = 0.05$.

3.3 Monte Carlo solver

The random continuous system is assessed by MC method (Shonkwiler and Mendivil, 2009). This stochastic solver uses a random number generator — a Mersenne twister pseudorandom number generator — (Matsumoto and Nishimura, 1998), to obtain many realizations of the random parameters of the system. In this work, many realizations of E are generated and each one of these realizations defines a new Eq.(4), so that a new variational problem is obtained. After that, these new variational problems are solved deterministically, such as in section 2.5. Then, the statistics of the random field U, such as the mean value and variance, are computed. More details about the MC method can be found in Liu (2001); Robert and Casella (2010).

4 NUMERICAL EXPERIMENTS

This sections presents numerical experiments performed with deterministic and stochastic models discussed above. The following physical parameters were adopted: $\rho = 7900\ kg/m^3$, $E = 203\ GPa$, $L = 500\ mm$, $A = 625\pi\ mm^2$, $k_1 = 1.3\times 10^7\ N/m$ and $k_2 = 5\times 10^{14}\ N/m^3$.

In addition, the initial displacement is given by

$$u_0(x) = \alpha \sin\left(\lambda_3 \frac{x}{L}\right) + \frac{x}{2000}, \tag{44}$$

and the initial velocity is identically zero, i.e.,

$$v_0(x) = 0, \tag{45}$$

for any $0 \le x \le L$. The constant $\alpha = 0.1\ mm$ is adopted.

4.1 Code verification test

The first experiment is a verification test (Oberkampf and Roy, 2010), to ensure the reliability of the code that implements the approximation proposed in section 2.4 and that is used the simulations reported in this work. In this test, one compares the approximation obtained with the code under verification with the analytical solution of the problem of section 2.2, when the nonlinear spring is not considered and the external force is assumed to be zero all over the bar at any time, i.e., $k_2 = 0\ N/m^3$ and $f(x,t) = 0\ kN/m$ for any $(x,t) \in [0,L]\times[0,+\infty)$. The analytical solution in question is given by

$$u(x,t) = \sum_{n=1}^{+\infty} a_n(t)\phi_n(x), \tag{46}$$

where ϕ_n are the orthogonal shape modes of the fixed-spring bar, Eq.(24), while

$$a_n(t) = C_n \cos\left(\lambda_n \frac{c}{L} t\right) + D_n \sin\left(\lambda_n \frac{c}{L} t\right), \tag{47}$$

C_n and D_n are given by

$$C_n = \frac{\displaystyle\int_0^L \rho A u_0(x)\phi_n(x)dx}{\displaystyle\int_0^L \rho A \left[\phi_m(x)\right]^2 dx} \qquad \text{and} \qquad D_n = \frac{\displaystyle\int_0^L \rho A v_0(x)\phi_n(x)dx}{c\lambda_n \displaystyle\int_0^L \rho A \left[\phi_m(x)\right]^2 dx}. \tag{48}$$

As can be seen in Figs. 3, 4, and 5, the developed code reproduces very well the solution of the code verification test case. The Figures 3(a) and 3(b) show the comparison of Galerkin and the analytical results for the essential boundary condition and the displacement initial condition, respectively. As can be seen, an excellent agreement is obtained. The Figures 4(a) and 4(b) show the evolution of the displacement of the right extreme of the bar, and the absolute error of the Galerkin approximation, defined as the absolute value of the difference between Galerkin approximation and the analytical solution. Note that the absolute error is almost always less than $\mathcal{O}(10^{-4})$ in semi-logarithmic scale. Figures 5(a) and 5(b) show the distribution of displacement of the bar at time $T = 4\ ms$ and corresponding absolute error, respectively. Note that, in semi-logarithmic scale, the absolute error is again almost always below $\mathcal{O}(10^{-4})$. Based on these results, one may conclude that the developed code successfully checked the functional verification test.

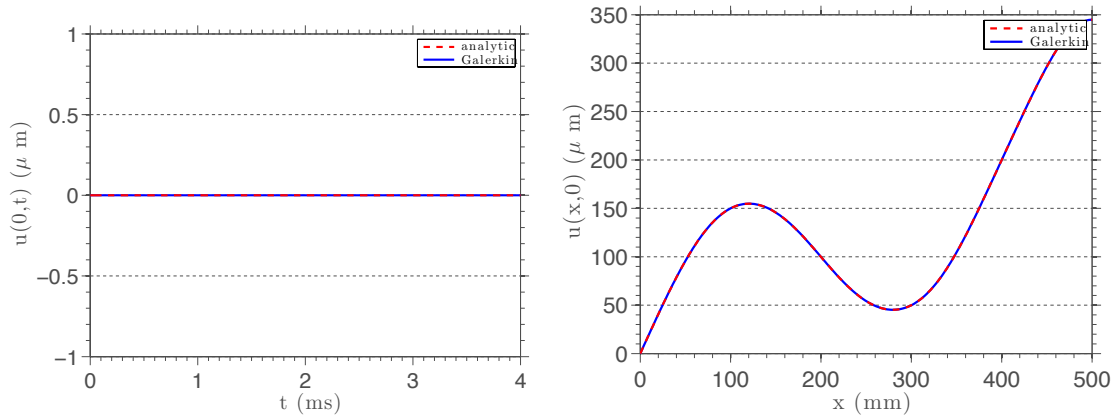

(a) Dirichlet boundary condition (b) Initial condition

Figure 3: Comparison between the analytical and Galerkin results, for initial and boundary conditions, in the code verification test.

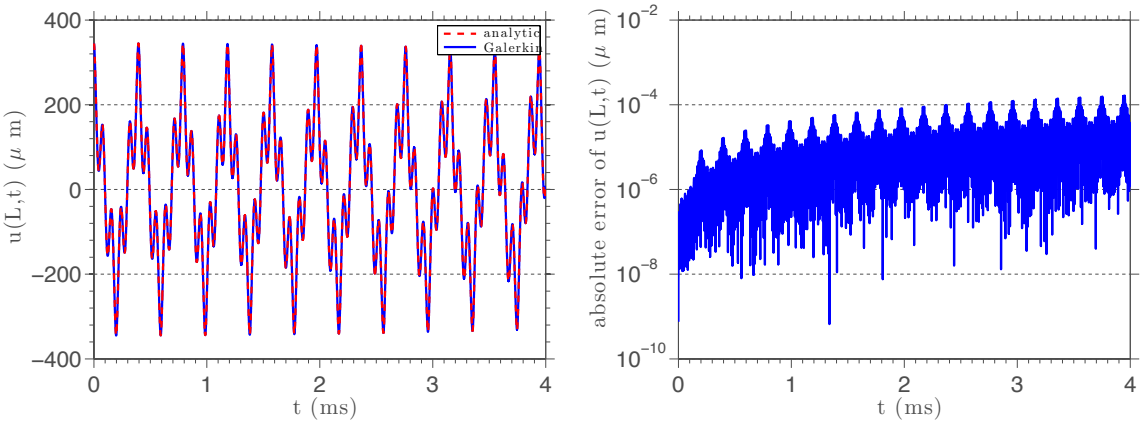

(a) (b)

Figure 4: Comparison between the analytical and Galerkin results for $u(L,t)$ and associated absolute error, in the code verification test.

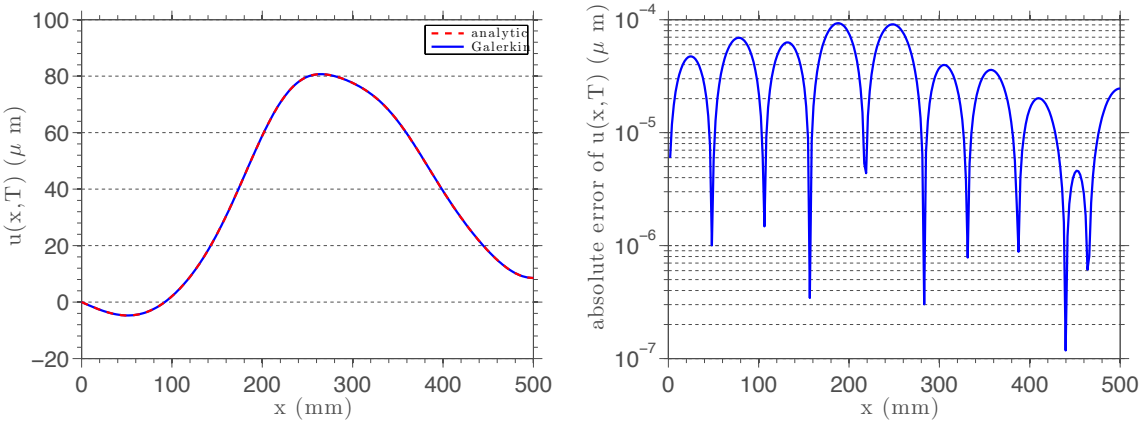

(a) (b)

Figure 5: Comparison between the analytical and Galerkin results for $u(x,T)$ and associated absolute error, in the code verification test.

4.2 Case 1: linear spring

The second numerical experiment (from now on called case 1) aims to study the dynamics of the fixed-spring bar, with a random elastic modulus, without the nonlinear spring, and subjected to a sine wave time-dependent external force with angular frequency equal to the first natural frequency, i.e., $k_2 = 0\ N/m^3$ and $f(x,t) = \sigma \sin\left(\lambda_1 \frac{x}{L}\right) \sin(\nu_1 t)$ for any $(x,t) \in [0,L] \times [0,+\infty)$ and $\sigma = 100\ kN/m$. The purpose of studying the dynamics of this linear random system is to obtain a reference dynamical behavior, for further comparisons with the nonlinear random system.

4.2.1 orthogonal shape modes of case 1

The first step of this study is to obtain number of shape modes necessary to correctly approximate the dynamics of the associated deterministic system. To quantify the error incurred by the approximation, two metrics are used. The first one considers the L_2 norm of the difference between two successive approximations; the other the H^1 norm of this difference. In this context, L_2 is the space of the square integrable functions and H^1 is a Sobolev space. The interested reader may consult Brezis (2010) for further details about these spaces and norms.

The results of the error measurements, with the number of shape modes varying from 5 to 30 units, are available in Tab. 1. A reduction of up to two orders of magnitude, is observed in the error measures. Analyzing these data, one can also observe that an approximation with 10 modes incurs an error of $\mathcal{O}(10^{-6})$ regarding the first norm and an error of $\mathcal{O}(10^{-4})$ considering the second norm. These values have an acceptable accuracy, such that all MC simulations of case 1 are performed using 10 orthogonal shape modes to construct the approximation.

Table 1: Study of convergence of the approximation, as function of the number of orthogonal shape modes, for case 1.

N	$\|\cdot\|_{L_2}$	$\|\cdot\|_{H^1}$
5	$\sim 8.06231 \times 10^{-5}$	$\sim 3.67343 \times 10^{-4}$
10	$\sim 9.94710 \times 10^{-7}$	$\sim 3.91851 \times 10^{-5}$
15	$\sim 2.91316 \times 10^{-7}$	$\sim 2.19139 \times 10^{-5}$
20	$\sim 1.27478 \times 10^{-7}$	$\sim 1.40486 \times 10^{-5}$
25	$\sim 7.68412 \times 10^{-8}$	$\sim 1.07035 \times 10^{-5}$
30	$\sim 5.67055 \times 10^{-8}$	$\sim 9.58419 \times 10^{-6}$

4.2.2 Monte Carlo simulations of case 1

The MC simulations of case 1 use 4^5 samples of the random variable E to characterize the random bar described in section 3 and compute its statistics, which are presented in Figs. 6 and 7.

In the Figures 6(a) it is shown the mean value of $U(L,\cdot)$, some realizations of this random process and an envelope of reliability, obtained using two standard deviations above and below the mean. One can observe an oscillatory behavior of the mean value of $U(L,\cdot)$. In addition, there is an increase in the amplitude of oscillation over time. This resonant behavior is due to external excitation frequency be equal to the first natural frequency of the bar. In the Figures 6(b) the reader can see the mean value of $U(L,\cdot)$ in details.

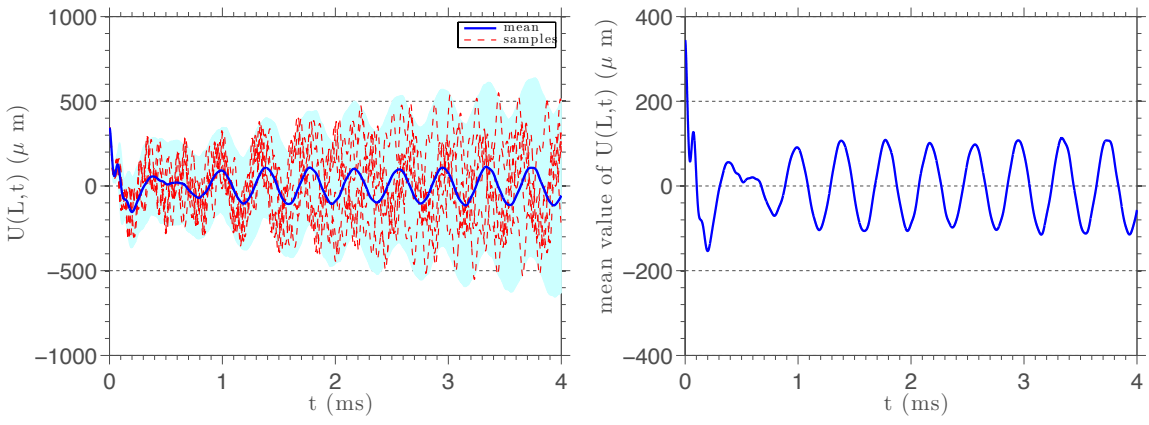

(a) (b)

Figure 6: The left figure illustrates mean value, some realizations and an interval of confidence (with two standard deviations) for the random process $U(L,\cdot)$ for case 1. The right figure shows, in details, the mean value of $U(L,\cdot)$.

In the Figure 7(a) the distribution of the mean value of $U(\cdot,T)$ is presented along the domain, some realizations of MC simulations, and an envelope of reliability similar to the one described above. While the Fig. 7(b) shows the mean value of $U(\cdot,T)$ in details. At first, the mean value of $U(\cdot,T)$ looks be zero, but looking Fig. 7(b) one can see that the mean value of $U(\cdot,T)$ have a strictly decreasing behavior along the domain. The shape of the confidence interval also allows one to see that the bar is vibrating in a configuration close to first orthogonal shape mode, which is natural once the external forcing has a $\sin\left(\lambda_1 x/L\right)$ term.

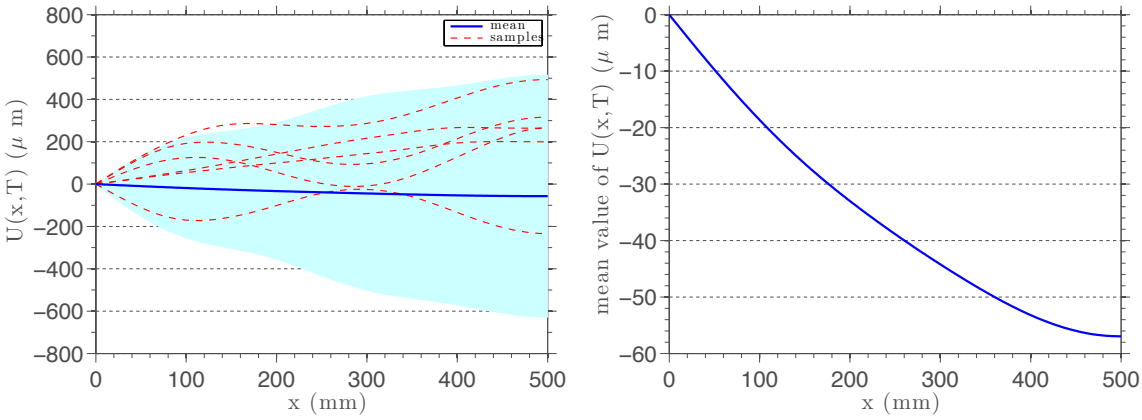

(a) (b)

Figure 7: The left figure illustrates mean value, some realizations and an interval of confidence (with two standard deviations) for the random field $U(\cdot,T)$ for case 1. The right figure shows, in details, the mean value of $U(\cdot,T)$.

4.3 Case 2: linear and nonlinear springs

The third numerical experiment (from now on called case 2) aims to study the dynamics of the fixed-spring bar, with a random elastic modulus, with linear and nonlinear springs, and subjected to a time-dependent external force similar to the one of case 2. Now the problem is nonlinear and the aim of the study is to characterize the changes in the system behavior induced by the nonlinearity.

4.3.1 orthogonal shape modes of case 2

In this case, the study of convergence of the approximation is done considering the nonlinear problem. The error induced by the approximation is quantified using the same metrics used in case 1, and the results of the error measurements are presented in Tab. 2. This table shows the convergence of the approximation as function of the number of orthogonal shape modes, again varying from 5 to 30. As in case 1, 10 modes give acceptable errors of $\mathscr{O}(10^{-6})$ in L_2 norm and of $\mathscr{O}(10^{-4})$ in H^1 norm. So, the MC simulations of this case are developed using 10 orthogonal shape modes.

Table 2: Study of convergence of the approximation, as function of the number of orthogonal shape modes, for case 2.

N	$\|\cdot\|_{L_2}$	$\|\cdot\|_{H^1}$
5	$\sim 1.38251\times10^{-4}$	$\sim 5.95130\times10^{-4}$
10	$\sim 2.34231\times10^{-6}$	$\sim 6.72901\times10^{-5}$
15	$\sim 5.14812\times10^{-7}$	$\sim 2.44444\times10^{-5}$
20	$\sim 2.43371\times10^{-7}$	$\sim 1.56991\times10^{-5}$
25	$\sim 1.45296\times10^{-7}$	$\sim 1.18598\times10^{-5}$
30	$\sim 1.00219\times10^{-7}$	$\sim 1.05516\times10^{-5}$

4.3.2 Monte Carlo simulations of case 2

The Figures 8 and 9 show, for case 2, the same information shown by Figs. 6 and 7 in case 1. Qualitatively, there is no difference between the results shown in Fig. 8 with respect those which are shown in Fig. 6. This indicates that the nonlinear spring has little influence on the evolution of the bar displacement at the extreme right.

As can be seen in Fig. 9, one notes that the consideration made on section 4.2.2 about the bar vibration configuration remains valid. This may imply that the nonlinearity does not change the system substantially. While a close inspection of Fig. 9(b) reveals that the mean value of $U(\cdot,T)$ changes its behavior drastically when compared with case 1. This is an evidence that the spring nonlinearity tends to affect more the spatial than temporal behavior of the bar.

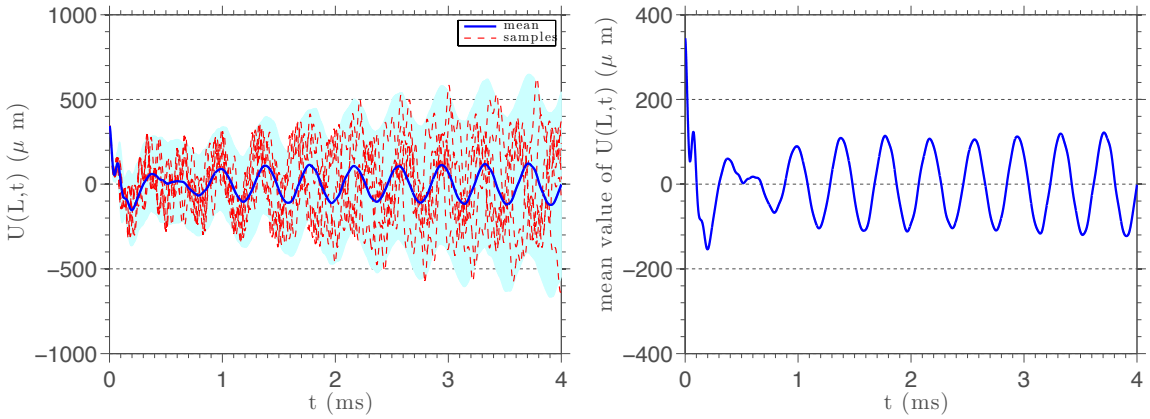

(a) (b)

Figure 8: The left figure illustrates mean value, some realizations and an interval of confidence (with two standard deviations) for the random process $U(L,\cdot)$ for case 2. The right figure shows, in details, the mean value of $U(L,\cdot)$.

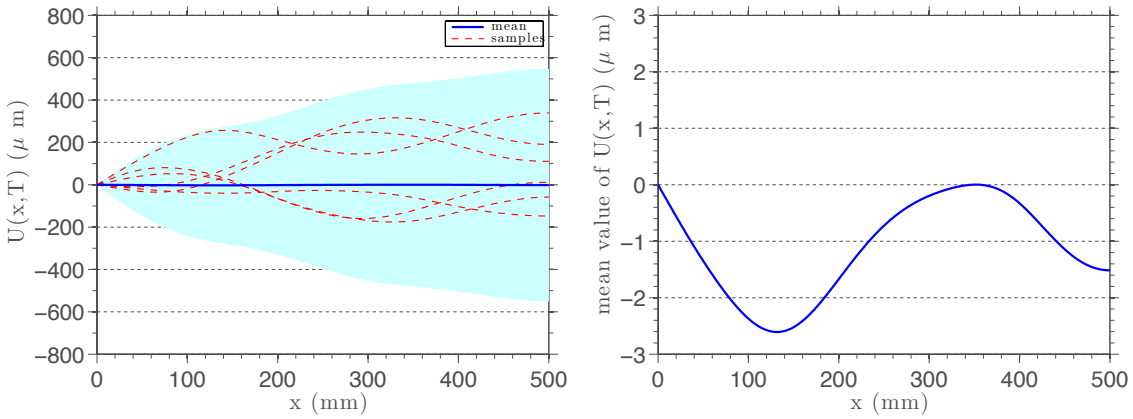

(a) (b)

Figure 9: The left figure illustrates mean value, some realizations and an interval of confidence (with two standard deviations) for the random field $U(\cdot,T)$ for case 2. The right figure shows, in details, the mean value of $U(\cdot,T)$.

The difference between the systems studied in cases 1 and 2 becomes even clearer if one looks to the histograms of Fig. 10, which represents the PDFs of the bar displacement at $x = L$ and $t = T$ for both cases. These histograms span approximately from -800 up to 800 μm, which corresponds to the range of displacement of the bar at $x = L$ and $t = T$.

The two distributions present discrepancies in various regions of the histogram. This provides another evidence for the thesis that the nonlinearity affects the bar spatial behavior. Since the only difference between one case to another is the nonlinear spring, it is natural to conclude that this discrepancy is due to the nonlinearity.

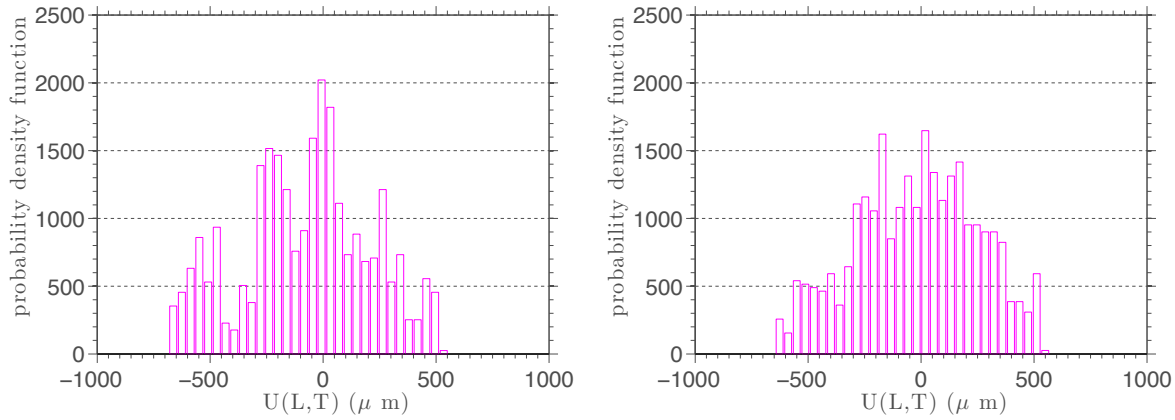

(a) case 1 (b) case 2

Figure 10: Comparison between the PDFs for $x = L$ and $t = T$.

5 CONCLUDING REMARKS

A model to describe the dynamics of a one-dimensional elastic bar, with a random elastic modulus, fixed in one extreme and attached to two springs (one linear and another nonlinear) also fixed at a rigid wall is presented. The strong and variational formulations of the deterministic case, as well as the procedure of discretization of the model equation and the iterative technique used to approximate the solution of the discretized equation are discussed in detail. The aleatory parameter is modeled as a random variable with gamma distribution, being the probability distribution of this parameter obtained by the principle of maximum entropy. The paper also analyzes two configurations of the bar model. The first configuration uses only the linear spring while the second one also considers the nonlinear spring. This analysis show that there are similarities and differences in the behavior of these two systems. The nature of the spring has little interference in the dynamics of the bar right extreme, but the nonlinearity affects significantly the spatial behavior of the bar. However, to better understand the nonlinear dynamics of this bar, further analysis are necessary.

For future works, one may suggests the development of other models for a elastic bar subject to nonlinearities and randomness. One possibility is to allow ρ and A vary throughout the domain. In this case the bar that is neither homogeneous nor its cross section area is constant. Another possibility is to consider the elastic modulus as a random field. Include in the model a random external force and/or change the boundary conditions could also be considered good options.

6 ACKNOWLEDGMENTS

The authors are grateful to Professors Mario Escalante (Universidad Tecnológica Nacional - Argentina), Olivier Le Maître (CNRS - France), and Thiago Ritto (UFRJ - Brazil), and to Dr. Julien Mauprivez (PUC–Rio) for valuable discussions and suggestions. The authors are also indebted to Brazilian Council for Scientific and Technological Development (CNPq) and Foundation for Research Support in Rio de Janeiro State (FAPERJ) for the financial support. Thanks also due to Cesar Augusto da Fonseca (PUC–Rio) and Professor Rui Pitanga Marques (CEFET/RJ - Brazil) who carefully revised the manuscript.

7 REFERENCES

Al Gwaiz, M. A., 2007, Sturm-Liouville Theory and its Applications. Springer, New York.

Blevis, R. D., 1993, Formulas for Natural Frequency and Mode Shape. Krieger Publishing Company, Malabar.

Brezis, H., 2010, Functional Analysis, Sobolev Spaces and Partial Differential Equations. Springer, New York.

Finlayson, B. and Scriven, L., 1966, The method of weighted residuals- A review, Applied Mechanics Reviews, 19 : 735–748.

Hughes, T. J. R., 2000, The Finite Element Method. Dover Publications, New York.

Jaynes, E. T., 1957a, Information theory and statistical mechanics, Physical Review Series II, 106 : 620–630.

Jaynes, E. T., 1957b, Information theory and statistical mechanics II, Physical Review Series II, 108 : 171–190.

Kapur, J. N. and Kesavan, H. K., 1992, Entropy Optimization Principles with Applications. Academic Press, San Diego.

Liu, J. S., 2001, Monte Carlo Strategies in Scientific Computing. Springer, New York.

Matsumoto, M. and Nishimura, T., 1998, Mersenne twister: a 623-dimensionally equidistributed uniform pseudo-random number generator, ACM Transactions on Modeling and Computer Simulation, 8 : 3–30.

Metropolis, N. and Ulam, S., 1949, The Monte Carlo Method, Journal of the American Statistical Association, 44 : 335–341.

Newmark, N., 1959, A method of computation for structural dynamics, Journal of the Engineering Mechanics Division, 85 : 67–94.

Oberkampf, W. L. and Roy, C. J., 2010, Verification and Validation in Scientific Computing. Cambridge University Press, New York.

Papoulis, A. and Pillai, S. U., 2002, Probability, Random Variables and Stochastic Processes. McGraw-Hill, New- York, 4th edition.

Robert, C. P. and Casella, G., 2010, Monte Carlo Statistical Methods. Springer, New York.

Shannon, C., 1948, A mathematical theory of communication, Bell System Technical Journal, 27 : 379– 423.

Shonkwiler, R. W. and Mendivil, F., 2009, Explorations in Monte Carlo Methods. Springer, New York.

Soize, C., 2000, A nonparametric model of random uncertainties for reduced matrix models in structural dynamics, Probabilistic Engineering Mechanics, 15 : 277 – 294.

Xiu, D. and Karniadakis, G. E., 2002, The Wiener-Askey Polynomial Chaos for stochastic differential equations, SIAM Journal on Scientific Computing, 24 : 619–644.

RESPONSIBILITY NOTICE

The authors are the only responsible for the printed material included in this paper.